

GPSSense: Passive Sensing with Pervasive GPS Signals

Paper #480

ABSTRACT

Wireless sensing, owing to its contact-free nature, is gaining increasing attention from both academia and industry. Various wireless signals, such as Wi-Fi, UWB, and sound, have been leveraged for sensing. While promising in many aspects, two critical limitations still exist: a) limited sensing coverage; b) and the requirement for dedicated sensing signals, affecting the original function of the wireless technology such as communication for Wi-Fi. To address these issues, we propose to utilize GPS signals for sensing, as they are already pervasive and emitted from satellites 24/7 within a pre-allocated frequency band, causing no interference. To make GPS sensing possible, we reconstruct the measurements reported by commercial GPS receiver modules into signals with amplitude and phase information which is critical for sensing. We also develop sensing models based on the unique features of GPS signals, such as their extremely long transmission distance. Finally, we introduce the concept of distributed sensing and design signal processing methods to fuse signals from multiple satellites to improve sensing performance. With all these designs, we prototype the first wireless sensing system based on GPS signals, called GPSSense, using commercial GPS receiver modules. We conduct comprehensive experiments to demonstrate that the proposed system can enable meaningful sensing applications such as human activity sensing, passive trajectory tracking, and respiration monitoring.

1 INTRODUCTION

Since Marconi's first wireless transmission in 1894, wireless technologies have progressively become an indispensable part of our everyday life. In addition to their primary communication function, exemplified by the prevalent Wi-Fi and 4G services [5], those wireless signals traditionally used for communication (e.g., Wi-Fi) have recently been explored for sensing purposes [22, 39, 41, 48]. The basic principle behind passive wireless sensing is that signal propagation gets affected by human motions and by analyzing the induced signal variations, the human's motion information can be inferred. The motions range from relatively large motions such as hand gestures [29, 46] to subtle motions such as respiration-induced chest movements [39, 44]. Basically, wireless signals rather than sensors are used for sensing purposes and the contact-free nature makes wireless sensing appealing in a lot of real-life scenarios. Diverse wireless signals have been exploited for sensing including Wi-Fi [26, 37],

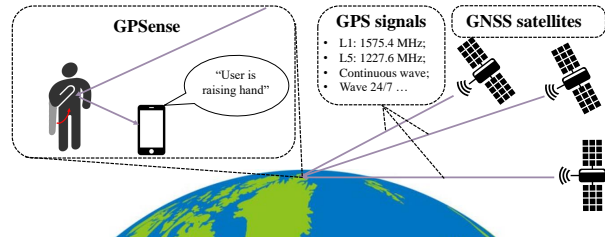


Figure 1: The sensing system based on pervasive and interference-free signals from GNSS satellites.

RFID [41, 52], mmWave [11, 21], UWB [46, 48], LoRa [39, 40], sound [19, 36] and Terahertz [3, 12]. While promising in many aspects, several issues still exist for current wireless sensing systems: i) The sensing coverage is still limited. The sensing coverage of one Wi-Fi AP¹ is just a few meters. ii) Dedicated sensing signals need to be transmitted which severely affect the original communication function. Take popular Wi-Fi sensing as an example. 200-1000 dedicated packets per second need to be transmitted for sensing [10, 42], which greatly degrade the data rate of ongoing data transmission.

To address the above challenges, the ideal wireless technology to be exploited for sensing is GPS (the Global Positioning System). One GPS satellite can cover 1/8 of the earth and 95% of areas on earth are covered by at least 4 GPS satellites [8]. Another unique advantage is that GPS satellites continuously emit signals 24/7. Therefore, no dedicated signals are required if we utilize GPS for sensing. Surprisingly, we did not find any research utilizing GPS signals for passive sensing (e.g., sensing the human's activities or tracking the human's moving trajectories). Note that passively tracking a human's moving trajectories using a static device placed a few meters away from the target is very different from actively tracking a GPS-equipped device moving together with the target to infer the human's moving trajectory. After we dig deeper, we find several challenges hindering GPS signals from being used for passive sensing.

- The first challenge is that most commercial GPS receiver modules do not report the information required for wireless sensing, i.e., the signal amplitude and phase information. Instead, only carrier-to-noise power density and pseudorange are reported.
- Existing wireless sensing models (e.g., the Fresnel zone model) do not apply to GPS signals due to the extremely long distance between the satellite and target, which is

¹Note that sensing coverage of WiFi is smaller than the communication coverage [44].

orders of magnitude larger than that of existing sensing modalities. What makes it even more challenging is that GPS satellites move at a high speed with respect to the human target on earth.² In comparison, Wi-Fi AP and LTE towers are stationary with respect to earth.

- There are many GNSS (global navigation satellite system) satellites on the Medium Earth Orbit (MEO) and GEO Geosynchronous Orbit (GEO). A GNSS receiver can receive signals from over 30 satellites at the same time from various GNSS satellites including GPS, Galileo (Europe) and BeiDou (China) moving at different speeds. As the navigation satellite moves faster than the earth's rotation, the satellites a receiver can capture signals from vary during a day. These factors make sensing using GPS signals and more generally GNSS signals more complicated than existing wireless sensing modalities.

To address the first challenge, we propose to reconstruct the original GPS signals including the amplitude and phase from the reported measurements to enable sensing. However, the reported measurements cannot be directly utilized for signal reconstruction due to inherent errors stemming from satellite movements and atmospheric delay [30]. We apply the satellite ephemeris data publicly available to address the error due to satellite movements and use the signal difference to mitigate the issue of atmospheric delay. However, after the errors are corrected, fully recovering the original signals is still challenging because the GNSS satellites also modulate encrypted messages on the signals [38]. Fortunately, for sensing, we do not care about the absolute signal amplitude and phase but rather the variation of signal amplitude and phase. Therefore, we do not need to obtain the absolute values of the signal parameters accurately but just need to make sure the signal format is correct and this is sufficient for us to extract signal variations for sensing.

To overcome the second challenge, we leverage the unique long propagation distance of GPS signals to develop the sensing model. Specifically, because of this long transmission distance, GPS signals from the same satellite can be treated as parallel waves with similar signal strengths upon reaching the sensing target and receiver. Building upon this fact, we develop two sensing models for GPS: the diffraction model and the reflection model. For the diffraction model, we adopt the Geometrical Theory of Diffraction (GTD) to analyze the interaction between such parallel signals and the blocking objects (human target). This model is independent of the transmitter location, and the movements of satellites only affect one variable in the model: the incident angle of the signal. This eliminates the need of knowing the transmitter's location in conventional wireless sensing models, which in our case keeps changing, for modelling. The transmitter's

location plays a key role in determining the Fresnel zones in the popular Fresnel zone sensing model [45]. For the reflection model, different from conventional wireless sensing models in which the signals reaching the target and the receiver are non-parallel, the GPS signals reaching the target and receiver can be considered parallel. What is more important is that the signal incident angle reported at the GPS receiver does not change with the target motion or target movement—a few meters of target motion is too small to change the incident angle due to the long signal propagation distance. This unique property is utilized to quantify the relationship between signal amplitude/phase variation and target movement.

To address the last challenge, we propose the distributed sensing concept leveraging the large number of satellites distributed at different locations on the orbits. We obtain multiple unique observations: i) The signals from satellites located on the *left (right)* side of the human target exhibit better performance for sensing *movements on the left (right) side of the body*; ii) The signals from satellites with *lower elevation angles* achieve a better performance for sensing *the movements of the target's lower body part (e.g., gait tracking)*. The signals with *higher elevation angles* achieve better performance for sensing *the movements of the target's upper body part (e.g., chest movement for respiration monitoring)*; iii) As GPS signals are parallel when they arrive at the Earth due to their extremely long transmission distance, the signals from satellites on the *same side* of the target with respect to the receiver will be influenced by the target's movements based on the *diffraction* model. Conversely, the signals from satellites on the *opposite side* of the target will be influenced by movements based on the *reflection* model. The information from multiple satellites is further fused to improve the sensing accuracy and robustness.

With all the challenges addressed, we realize GPSense, the first passive wireless sensing system based on GPS signals. Without any hardware modifications, GPSense is able to achieve an accuracy of 94% in recognizing eight human activities. Besides, it can also achieve device-free trajectory tracking and respiration monitoring.

We conduct comprehensive experiments to validate the system's robustness under various conditions including different time of a day, different weather conditions, different targets, and diverse environments. We also successfully make the proposed GPS sensing work in indoor environments with the help of a cheap GPS repeater (\$3.5) [1]. GPSense is implemented on multiple mainstream GPS receiver modules used in smartphones, and smartwatches. To summarize, we make the following contributions:

- We are the first to harness GPS and more general GNSS signals for passive sensing, wherein the target does not

²The GPS satellite moves faster than the earth's self rotation.

- carry a GPS (GNSS) receiver. We believe this new sensing modality enables truly wide-area wireless sensing which will trigger a large range of new sensing applications.
- As sensing just cares about signal amplitude/phase variations rather than the absolute readings, we utilize the reported high-level measurements from commercial GPS modules to reconstruct the GPS (GNSS) signals which are not exactly the same as the original ones but are sufficient for sensing.
 - Based on the unique characteristics of GPS signals, we present two sensing models tailored for GPS sensing. These models quantify the relationship between the target movement and corresponding signal variations, laying the theoretical foundation for GPS sensing.
 - Based on the unique observations such as the satellites with higher elevation angles are more suitable for sensing the upper part of the human body, we propose the concept of distributed sensing to fuse signals from multiple satellites to improve the sensing performance.
 - We implement GPSSense on commercial GPS receiver modules and validate the system's effectiveness and robustness with representative sensing applications (i.e., activity recognition, trajectory tracking, and respiration monitoring) under various conditions. We also show that with a cheap GPS repeater (\$3.5), we can extend GPS sensing to indoor environments.

2 GPS SIGNAL PRELIMINARY

We take the Global Positioning System (GPS) as the example to introduce the Global Navigation Satellite System. GPS comprises 31 satellites on the medium Earth orbit, continuously emitting Radio-Frequency (RF) signals to facilitate navigation functions for billions of devices. Smartphones, drones, and vehicles can receive these signals and determine their Earth positions through triangulation. The triangulation method requires target devices to receive signals from a minimum of four GPS satellites. Signals from multiple satellites are available nearly anywhere and at any time. Besides, to prevent interference with existing communication services such as Wi-Fi, LTE, and Bluetooth, GPS transmits signals at central frequencies of 1575.42 MHz and 1227.6 MHz. Therefore, GPS signals possess the potential as sensing signals for pervasive coverage and at the same time do not affect existing data communication.

To optimize computational resources and minimize data transmission cost, GPS receiver modules embedded in commercial devices typically only report processed measurements. These measurements are directly computed by the processing chip in the receiver module, utilizing the original GPS signals received, and subsequently sent to the device's

processing unit. The most frequently reported measurements are summarized as follows:

Carrier-to-Noise Power Density (C/N0). This measurement measures the ratio of the power level of a signal carrier to the noise power in a 1-Hz bandwidth [17]. This is a key parameter in the analysis of GPS receiver performance. This measurement can be expressed by

$$C/N_0 = 10 \log_{10} \left(\frac{P_c}{P_n/B} \right), \quad (1)$$

where P_c is the power of the GPS carrier, P_n is the power of the noise floor and B is the bandwidth.

Pseudorange. The pseudorange is a time-of-flight measurement calculated using the *Coarse Acquisition (C/A)-Code*, which corresponds to the distance between the receiver antenna and the satellite antenna, including the receiver and satellite clock offsets and other biases such as atmospheric delays. Pseudorange ρ can be expressed as

$$\rho = r + ct_b + \varepsilon_\rho, \quad (2)$$

where r is the geometric range between the receiver and the satellite, c is the light speed, and t_b is the clock bias of the receiver.

Accumulated Carrier Phase. Commercial GPS receivers can acquire the accumulated carrier phase as a measurement, which keeps accumulating since the GPS receiver starts. The carrier phase measurements Φ can be expressed by

$$\Phi = r_0 + \int_0^t 2\pi f_D dt + \varepsilon_\Phi, \quad (3)$$

where f_D is the phase caused by Doppler frequency, r_0 is the initial geometric range between the receiver and the satellite, and ε_Φ is the measurements errors. Note that phase measurements in some GPS receiver systems are reported in meters. For example, Android Smartphones report the carrier phase measurements as *Accumulated Delta Range*, which is actually $\lambda\Phi$.

These measurements play a pivotal role in the navigation application of the commercial device, enabling the computation of its precise location.

3 GPSENSE MODEL

In this section, we take the GPS signal as the example to illustrate how to reconstruct the original signals based on the processed measurements. Then we present the two sensing models for GPS signals.

3.1 GPS Signal Reconstruction

As mentioned in Sec. 2, the commercial devices can only access the processed measurements from the GPS module, and these measurements can not be directly used for sensing due to multiple reasons: a) Measurement errors. Errors are caused by various factors such as weather and clock drift

during the long-range (about 20000 km) propagation. The signal variation caused by the sensing target can be buried by the variation caused by the errors without being detected. b) Coarse channel state information: the measurements are reported for calculating the distance between satellites and the receiver and the measurements are too coarse to be utilized for fine-grained sensing (e.g., respiration monitoring). For example, the distance resolution with a single satellite based on these measurements is about 300 m. To extract the fine-grained channel state variation for sensing, we design a *signal reconstruction scheme* to reconstruct the original GPS signals using the reported GPS measurements.

Measurement error correction. In this step, we preprocess the GPS-reported measurements to eliminate errors during the long-range propagation. Specifically, there are two factors that cause errors in the GPS measurements including a) movements of the satellites; b) clock error of the GPS receiver. All these factors should be addressed properly to reduce their influence on reported measurements for sensing.

First of all, to eliminate the influence of GPS movements, we explore the publicly accessible ephemeris data, which reports the real-time locations of the satellites every 15 minutes. We use the satellite's location and orbit information to estimate the movement status of each satellite. After we obtain the movement status of the satellite, we calculate the effect of Doppler shift on the signal phase caused by the movement, and then we compensate the phase error caused by Doppler (f_D) in the accumulated carrier phase measurements. To mitigate the effect of clock errors on pseudorange (t_b), we employed the weighted least squares algorithm [17]. This method involves simultaneous utilization of multiple synchronized satellites to calculate the clock bias between the satellites and the receiver, enhancing the precision of the measurements [25].

Basic signal parameter calculation. In the second step, we combined these pre-processed measurements to calculate the basic signal parameters, i.e., amplitude $Amp(t)$ and phase $\phi(t)$. Then, the GPS signal is reconstructed for sensing. $Amp(t)$ can be estimated as

$$Amp(t) = \sqrt{P_n 10^{(C/N_0)/10}}, \quad (4)$$

where $P_n = kT$ is the noise power in a 1-Hz bandwidth [17], k is the Boltzmann constant in Joules per Kelvin, T is the temperature in Kelvin, C/N_0 is the reported Carrier-to-Noise Power Density, which has been corrected in Step 1. The carrier phase ϕ of the GPS signal can thus be expressed as

$$\phi(t) = \left(\frac{d\Phi}{\lambda dt} - \frac{2\pi f_D t}{\lambda} \right) + \frac{\|\rho - ct_b\|}{\lambda}, \quad (5)$$

where Φ is the reported accumulated carrier phase, ρ is the reported pseudorange, f_D is the phase error caused by the Doppler effect from the satellite movement, t_b is the clock bias of the receiver, all of which were estimated already in

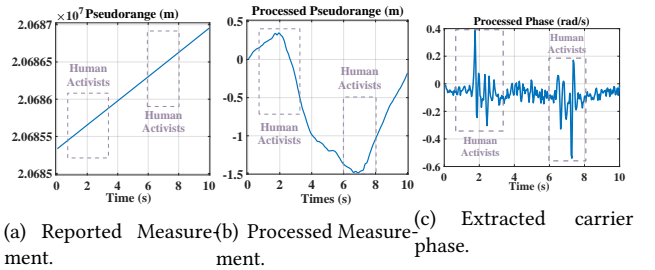


Figure 2: Signal comparison among the reported measurement, processed measurement, and the extracted signal feature.

Step 1. After obtaining the amplitude and phase values, we can reconstruct GPS signal at timestamp t as

$$S(t) = Amp(t)e^{j\phi(t)}. \quad (6)$$

To demonstrate the sensing capability of the reconstructed GPS signal, a benchmark experiment is conducted, wherein a human target is asked to move around the GPS receiver module, inducing variations in the received signals. Figure 2 depicts the reported pseudorange, the corrected pseudorange and the reconstructed signal phase. It is evident that the reported pseudorange does not contain meaningful information due to the aforementioned measurement errors. Moreover, even with the correction of the reported pseudorange, its signal variation fails to show the fine-grained channel changes induced by the target's movement around the receiver, as the pseudorange measurement is designed for coarse-grained distance estimate. Ultimately, our proposed method successfully yields fine-grained signal phase variations due to the target's movement. Without loss of generality, we employ these reconstructed signals to represent the received GPS signals in subsequent sections for sensing. Besides, the reconstruction process is similar for other GNSS satellites such as BeiDou.

3.2 The Reflection of GPS Signals

After reconstructing the GPS signals from the reported measurements, we proceed to establish the correlation between signal variations and target movements for sensing. The conventional sensing models, e.g., the Fresnel zone model [45], are not suitable for GPS signals due to the extremely long signal propagation distance and constantly moving satellite at a speed of 4 km/s. In this section, we model the reflection of GPS signals and quantify the relationship between target movements and the induced signal variations. We analyze the model theoretically and validate its effectiveness through experiments.

Modeling the reflection from a moving object. The comprehensive signal reflection model for stationary objects is presented in the Appendix and we focus on the reflection model for moving objects. As shown in Figure 3, a target

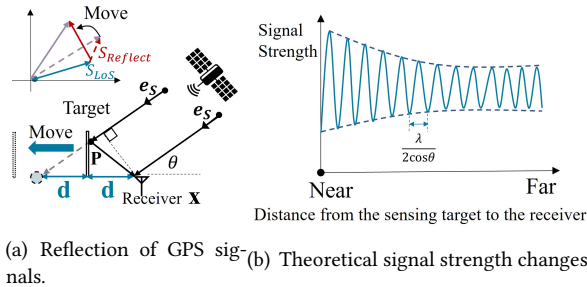


Figure 3: A moving object moving away from the LoS between the satellites and the GPS receiver.

moves forward and backward towards the LoS path between a satellite and a receiver. The receiver captures signals from both LoS path and reflection from the target. The horizontal distance (d) from the GPS receiver to the target can be expressed as

$$d = \|\mathbf{x} - \mathbf{p}\| \cdot e_s = \|\mathbf{x} - \mathbf{p}\| \cos\theta, \quad (7)$$

where \mathbf{x} is the receiver location, \mathbf{p} is the reflection point, e_s represents the GPS signal, and θ is incident angle of the GPS signal. Then the phase difference between the LoS signal S_{LoS} and reflection signal $S_{Reflect}$ can be simplified as

$$\phi_{Reflect} - \phi_{LoS} = \frac{2d\cos\theta}{\lambda} + \pi, \quad (8)$$

which is linearly related to the distance d as the elevation angle of the satellite is a constant in a short time window (e.g., 10 s). Due to the constructive and destructive combination between the LoS signal and the reflection signal illustrated in Figure 3(a), the signal will manifest repetitive peaks during the process of target movement, as demonstrated in Figure 3(b). Based on Equation 8, we know the interval between adjacent two peaks is $\frac{\lambda}{2\cos\theta}$, allowing us to deduce the distance of the target's movement by measuring the number of observed peaks. The peak signal strength decreases as the target moves further away from the receiver.

We conduct a benchmark experiment to verify the theoretical observation. We place a metal box on a sliding rail and move it away from the receiver. We then measure the distance between two adjacent peaks to validate our model. As shown in Figure 4 (b), We plotted the measured GPS signal strength from satellite G19. The average of measured moving distances between two peaks is 0.105 m, which well matches the theoretical distance (0.101 m) based on Equation (8). For this reflection model, only the reported signal incident angle is required for sensing without a need of knowing the satellite's detailed status such as moving speed and direction.

Reflection from the human body. In the reflection model, the received signal at the receiver contains both the reflection signal and LoS signal. However, due to the weaker signal (-120 dBm) compared to other wireless signals such as

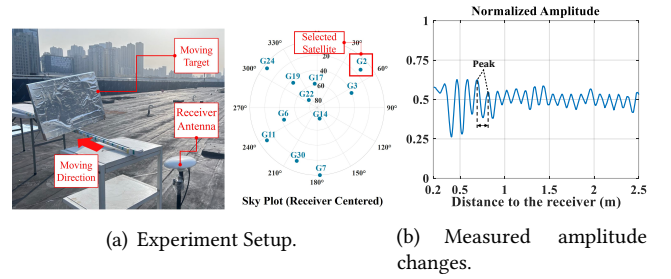


Figure 4: Reflection Verification Experiment: a metal box moving away from the GPS Receiver.

Wi-Fi, the GPS reflection signal can only be detected when reflected from a relatively large body part, such as the torso. The weaker reflection signals from arms are hard to be detected. To sense arms and legs, signals from other satellites which are influenced by the diffraction effect can be used. Detailed results of experiments on tracking, localization, and activity detection will be presented in Section 5.

3.3 The Diffraction of GPS Signals

In this section, we present the diffraction model for GPS sensing to quantify the effect of motion activities on signal variations. Both theoretical analysis and experiment are employed to validate the proposed model.

Modeling the diffraction effect caused by a moving object. The diffraction effect dominates when the human target is very close to or on the LoS path of the GPS signal. When a GPS signal wave impinges on the edge of an object (e.g., a human target), Keller's Geometrical Theory of Diffraction (GTD) [15] depicts the occurrence of outgoing rays in the shape of a cone. The Keller Cone model for stationary objects is presented in the Appendix, and we focus on the case of moving objects for sensing.

As shown in the Figure 5 (a), considering a scenario that a target moves across the LoS between a GPS satellite and a GPS receiver, GPS signals get diffracted at the edge of the moving target. Before the front edge of the target reaches the LoS path, the measured signal strength is roughly constant as shown in Figure 5 (b). When the target moves further, the object's Keller Cone due to diffraction appears. Now the GPS receiver receives a combination of the diffracted GPS signals and the LoS signal, causing a small variation of the combined signal strength as the LoS path signal still dominates. When the target moves further and the LoS path is obstructed, the strength of the received signal decreases rapidly. During the process of moving across, the signal strength fluctuates. As shown in Figure 5, when a GPS receiver is located at different locations, the signal strength fluctuation pattern varies. When the GPS receiver is deployed at location 1, two peaks appear on the signal strength plot during the process of targeting cutting the LoS path. When the receiver

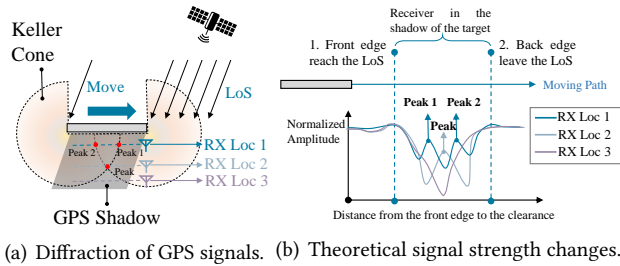


Figure 5: A moving object moving across the LoS between the satellites and the GPS receiver.

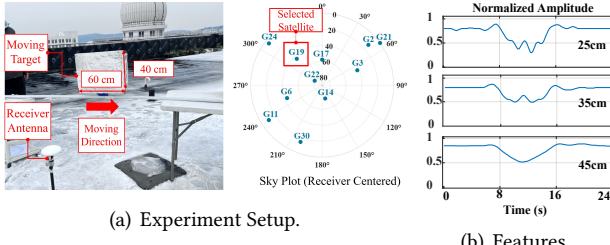


Figure 6: Diffraction Verification Experiment: a metal box moving across the LoS between the GPS Receiver and a GPS satellite.

is at location 2, only one peak appears. At location 3, due to destructive combination, only one valley can be observed.

We conduct experiment to see the signal variation when an object moves across the LoS path between the satellite and the GPS receiver. As shown in the Figure 6 (a), we employ a metal box as the object and the G19 satellite as the transmitter. The elevation angle of the satellite is about 43 degrees. When we place the GPS receiver at a distance of 25 cm, 35 cm and 45 cm away from the target moving trajectory, we obtain three plots (i.e., two peaks, one peak and one valley) as shown in Figure 6 (b) which match the theoretical analysis in Figure 5 well.

The diffraction of the human body. The human body causes rich diffraction when the body is near to or on the LoS path [45]. Based on the analysis and experiments in previous sections, the GPS signal variation pattern can be leveraged to infer the size of the target. The target movement directions can also be acquired when we use multiple satellites to sense, which will be detailed in Section 4.

4 GPSENSE DESIGN

We have established the basic sensing model for the proposed system based on the GPS signal from a single satellite. There are over one hundred GNSS satellites currently in use, including GPS, BeiDou, etc. The signals from all these satellites can be utilized for our sensing tasks. This brings the concept of distributed sensing and we leverage signals from multiple satellites to improve the sensing performance in terms of

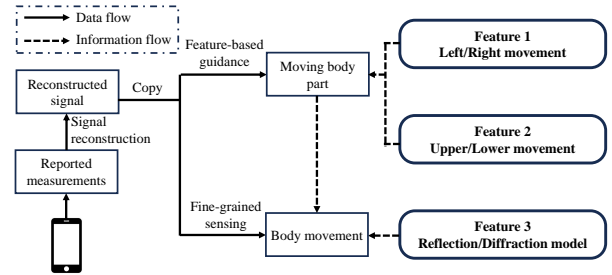


Figure 7: System pipeline

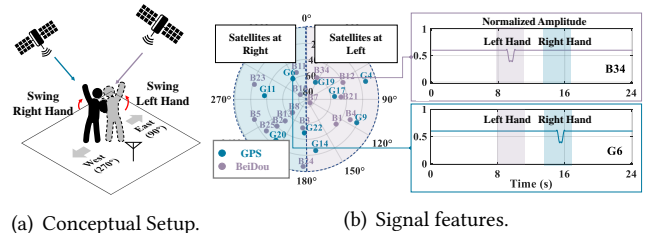


Figure 8: Combine the GPS signals with satellites from different azimuth angles.

sensing accuracy and sensing robustness. However, as GNSS satellites are positioned in the medium Earth orbit and move faster than the earth self rotation, the GPS signals received at the same device are from different satellites at different time of day. It is thus important to dynamically select satellites as the signal sources for sensing. In this section, we also introduce the unique features of GPS signals and leverage them for sensing. The signal processing pipeline is presented in Figure 7.

4.1 Sensing with Multiple Satellites

Based on the two sensing models introduced in Section 3, we pinpoint three features regarding the sensing capability of GPS signals related to satellite positions. Benchmark experiments are employed to validate the identified features.

Feature 1: Satellite on the right/left of the target. The first factor influencing the GPS signal's sensing capability is the azimuth direction of the satellite. Based on the established sensing models, signals transmitted from satellites positioned to the right of the sensing target have a higher probability of undergoing diffraction or reflection effect caused by the right side of the body. Consequently, variations in these signals contain more information of movements on the right side of the target. As illustrated in Figure 8, it follows that signals emitted from satellites located on the *right side* of the target exhibit superior sensing capability for *movements on the right side of the body*. Similarly, signals from satellites positioned on the *left side* can better sense *movements on the left side of the body*.

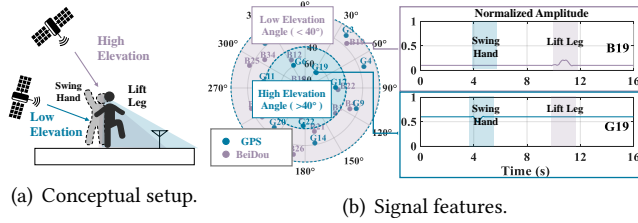


Figure 9: Combine the GPS signals with satellites from different elevation angles.

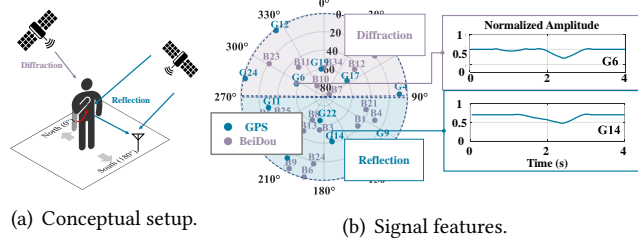


Figure 10: Combine the reflection and diffraction GPS signals.

As depicted in Figure 8(a), the target faces the GPS receiver in a direction of 180° (South). The target first waves her left hand and then waves her right hand. Figure 8(b) displays the sky plot at the specified timestamp and the signal variations from satellite B34, positioned to the left of the subject, and satellite G6, positioned to the right of the subject. It is evident that when the subject waves her left hand, it solely affects the signals from satellites positioned to their left, and similarly when waving her right hand.

Feature 2: Satellite at high/low elevation angle. Another feature influencing the sensing capability of GPS signals is the elevation angle. As illustrated in Figure 9(a), signals from satellites with *higher elevation angles* show superior sensing capability for *upper body movement*, whereas signals from satellites with *lower elevation angles* excel in sensing *lower body movement*.

We conduct an experiment to validate this feature, as depicted in Figure 9(a), where the subject first swings her hand and then lifts her leg. The signal variations during the process of the movements are shown in Figure 9(b). When the subject swings her hands, the signals from a satellite at a high elevation angle (B19) experience significant influence, while signals from a satellite at a low elevation angle (G19) remain relatively stable. This suggests that the upper body of the subject is in motion while the lower part remains static. Similarly, the movement of lifting leg tends to affect the GPS signals from a satellite with a lower elevation angle (B19) rather than a satellite with a higher elevation angle (G19).

Feature 3: Satellite at same/opposite side of the target. Due to the extremely long transmission distance of GPS signals, they are parallel when they arrive at the target and receiver. When the satellite and the target are at the *same side*

with respect to the target (Satellites in the north in Figure 10), GPS signals will be influenced by *diffraction*. When the satellite and the target are at the *opposite side* with respect to the receiver ((Satellites in the south in Figure 10)), the signal variation is contingent upon the *reflection*.

We conducted an experiment to validate this feature. The experimental setup is depicted in Figure 10(a), where the subject puts her hand to the chest and then puts it back. We plotted the satellite sky-plot during the experiment and the signal variations from two selected satellites, namely G6 and G14 as shown in Figure 10(b). Based on the geo-location relationship, for G6, diffraction model should be applied and for G14, reflection model should be applied. As depicted in Figure 10(b), both models can sense the target's motion. This shows the capability of the proposed system to concurrently employ both models for sensing.

4.2 Feature-based sensing design

Based on the described features, we propose to combine these features for device-free activity recognition. While we employ activity recognition to illustrate the concept, our system can be applied for other sensing applications such as respiration monitoring and device-free trajectory tracking which will be demonstrated with experiments in 5.

A GPS receiver can receive GPS signals from multiple satellites present in the current sky. We can thus generate a sky plot as depicted in the left one of Figure 11. Then, we identify which part of the target's body is moving by comparing signal strength variations caused by target movement at different satellites using Feature 1 and 2. Take the example of one target waving her left hand. We first compare the average signal variation from satellites on the left side with that from the right side. If the value from the left side is higher, our system concludes that the movement is from the left side of the target, and vice versa. In the current scenario, with larger left-side signal variations, we only consider GPS signals from the left side as shown in Figure 11. Similarly, the system further compares the average signal variation at high elevation angles with that at low elevation angles. The elevation angle threshold is set at 40° as illustrated in Figure 11. We observe that the average signal variation at high elevation angles exceeds that at low elevation angles. The system thus deduces that the current movement pertains to the upper body part of the target based on Feature 2.

4.3 Fine-grained Activity Sensing

We employ dynamic time warping (DTW) to compare the collected signal sample with the one stored in the database for fine-grained activity recognition. However, the crucial aspect lies in how we combine GPS signals from multiple

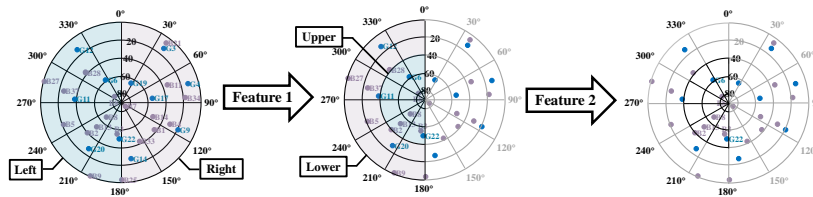


Figure 11: Combine the GPS signals based on Feature 1&2.

remaining satellites after the feature-based guidance for sensing. We still employ the example of the target waving her left arm to elaborate the concept. For reference (database) signal collection, the target is only required to perform the movement once as the collected GPS signal contains data from all satellites present in the sky at that specific timestamp.

Combining the reflection and diffraction model. After we know the basic information of the movement (e.g., left-side upper-body movement), we can apply Feature 3 to tell if the signal from a particular satellite experiences diffraction effect or reflection effect. The reference sample is denoted as $X_r^D(i)$, where $i \in N$ and N represents the number of left-side upper-body movement types. Similarly, the reference sample for each movement based on the reflection model is denoted as $X_r^R(i)$, where $i \in N$. Following that, we designate the current sample for the diffraction model as x_c^D , selected from the received GPS signals with the largest variation. Similarly, the current sample for the reflection model is denoted as x_c^R . The dynamic time warping (DTW) method is then applied as follows:

$$\arg \min_{i \in N} ||x_c^D||^2 \text{DTW}(x_c^D, X_r^D(i)) + ||x_c^R||^2 \text{DTW}(x_c^R, X_r^R(i)). \quad (9)$$

Here, $||x_c^D||^2$ and $||x_c^R||^2$ represent the signal variance for the current sample based on the diffraction and reflection models, respectively. These are multiplied as weights to the corresponding DTW results.

However, the GNSS satellites are constantly moving. Although we have compensated for the influence of the satellite movement on signals in Section 3, the satellite positions during the collection of the current sample differ from those during the collection of the reference sample. Even for the same movement, GPS signal variations for satellites at different positions remain distinct. Thus, the signal variations depend not only on target movement but also on satellite's positions, rendering the basic DTW method ineffective.

To address this issue, we leverage the observation that *the signal variations for satellites within a azimuth and elevation angle range exhibit similar patterns for the same target movement*. Based on our experiments, the angle range is 30 degrees for azimuth angle and 10 degrees for elevation angle. Thus, we subdivide the sky plot into smaller sectors based on this minimum azimuth and elevation angle range as shown in Figure 12. This ensures that within the same

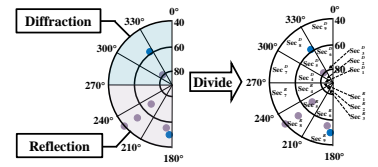


Figure 12: Combine two models and sector division.



Figure 13: GNSS Module.

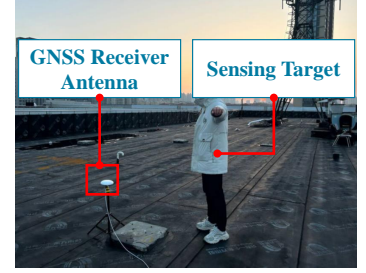


Figure 14: Default Setup.

angle sector, the signal patterns of different satellites for the same movement remain consistent.

When collecting the reference sample for a specific movement, we divide satellites based on angle sectors and select the signal with largest signal variations in each sector, denoted as $X_{rj}^R(i)$ and $X_{rj}^D(i)$, where $j \in M$, $i \in N$, and M represents the number of sectors. Note that the user is required to perform each movement only once for reference sample collection. Additionally, we allocate a weight to each sector, where the weight for each sector is denoted as $W_j^R(i)$ and $W_j^D(i)$, where $j \in M$, $i \in N$. While the current sample is a set of largest signal variations in different sectors as x_c^R and x_c^D , where $j \in M$. The complete algorithm to classify the current sample into the specific movement is as follows:

$$\begin{aligned} \arg \min_{i \in N} & \sum_{j \in M} ||x_c^D||^2 W_j^D(i) \text{DTW}(x_c^D, X_{rj}^D(i)) \\ & + \sum_{j \in M} ||x_c^R||^2 W_j^R(i) \text{DTW}(x_c^R, X_{rj}^R(i)). \end{aligned} \quad (10)$$

5 EVALUATION

5.1 Implementation

In this section, we introduce the implementation of GPSense. As depicted in Figure 13, we use the Ublox F9P GNSS module as the default receiver with a update rate of 25 Hz. We test GPSense on various commercial GNSS receivers with update rates ranging from 1 Hz to 25 Hz to confirm its broad applicability. For processing signals, we employ a laptop equipped with an Intel i7 CPU and 16 GB of memory. The standard setup, as depicted in Figure 14, is simple: a GNSS receiver is positioned on the ground or roof while the target performs activities or moves around nearby.

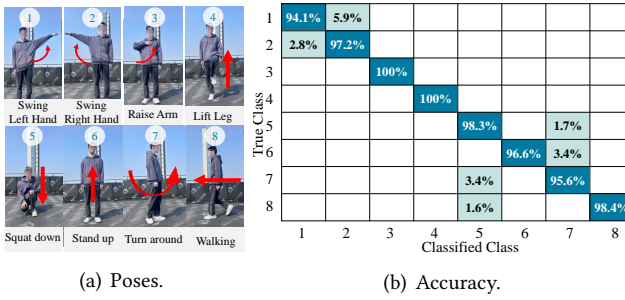


Figure 15: Overall Body Postures.

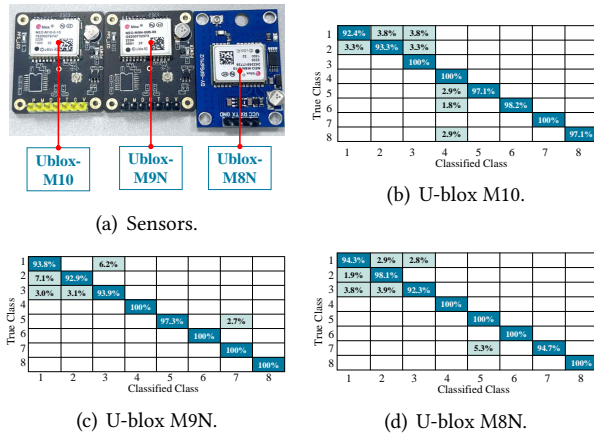


Figure 16: Sensing accuracy with different GNSS receiver modules.

5.2 Human Activity Sensing

In the first experiment, we ask a volunteer to perform eight different body movements as shown in Figure 15 (a) to evaluate the GPSense’s sensing accuracy for human activities. For each activity, the target repeats the movement 100 times, while we take one of the samples as the reference. Figure 15 shows that the sensing accuracy for these eight activities is about 97.6%. Moreover, we notice that some activities such as raising the arm cause changes on both reflection and diffraction features. This observation supports our approach of combining reflection and diffraction models for sensing.

Sensing with different GNSS receiver modules. We implement GPSense on multiple other commercial GNSS receiver modules, as depicted in Figure 16(a), and conduct experiments to evaluate their performance. These modules are commonly found in smartwatches (e.g., Ublox M10 [2]), smartphones (e.g., Ublox M9N [31]), robots, and unmanned aerial vehicles (e.g., Ublox M8N [32]). In each experiment, the target repeats the same eight movements as in the previous section with different GNSS receiver modules. These modules operate at the default sampling rate of 10 Hz, 25 Hz, and 15 Hz to collect GPS signals. The respective sensing results

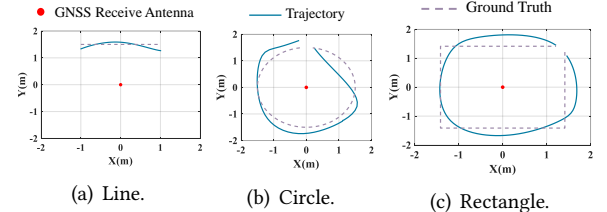


Figure 17: Passive trajectory tracking.

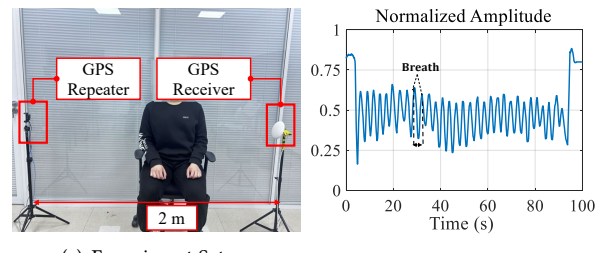


Figure 18: Breath Counting with GPS signals.

are presented in Figure 16(b), Figure 16(c), and Figure 16(d), with an average sensing accuracy of 97.3%, 97.2%, and 97.4%, respectively, which are similar to the sensing accuracy of the default GNSS receiver (97.6%). These results demonstrate that our system can readily be deployed on commercial GNSS receiver modules.

5.3 Passive Trajectory Tracking

In addition to activity sensing, our system can achieve passive trajectory tracking for the target near the GNSS receiver. Our system does not require the target to carry any receiver. Instead, it induces the trajectory by analyzing signal variations caused by target moving, distinguishing it from traditional GPS tracking. We ask a volunteer to walk along the pre-defined trajectories, including a straight line, a circle and a rectangle near the GNSS receiver as shown in Figure 17(a). The key principle behind trajectory tracking is that the human’s working affects the LoS paths of different satellites temporally. Our system can achieve decimeter-level passive trajectory tracking, as shown in Figure 17.

5.4 Contact-free Respiration Monitoring

The proposed system can also be used to monitor subtle vital signs of the target, i.e., respiration. Since respiration monitoring typically happens in indoor environments, we employ a low-cost GPS repeater (\$3.5) to bring GPS signals into the room [7]. The experiment setup is illustrated in Figure 18(a), where the repeater is deployed 2 m away from the GNSS receiver. Then we ask a volunteer to sit between the GPS repeater and the receiver with the chest close to the LoS path.

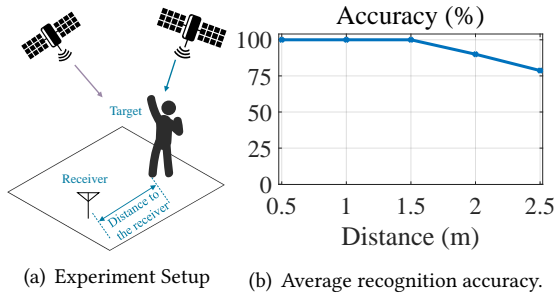


Figure 19: The recognition accuracy with respect to distance changes.

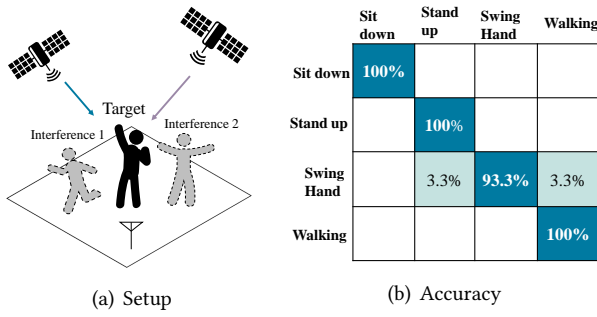


Figure 20: Other volunteers as inference.

We instruct the user to breathe naturally 30 times and use the GNSS receiver to collect signals during the process. The extracted signal amplitude variations, resulting from the proposed signal reconstruction method, are plotted in Figure 18(b). We can see that each peak and valley pair corresponds to one respiration cycle, with 30 peaks and valleys clearly observed. Furthermore, we instruct the volunteer to breathe naturally for 90 seconds and count the number of breath cycles. We repeat the experiment ten times. The achieved average respiration rate estimation error is 0.6 respiration per minute, which falls in category of good performance [43].

5.5 Sensing Capabilities

In this section, we further explore the performance boundary of GPSense, including the sensing coverage and multi-target sensing. We choose four representative human activities, i.e., walking, vertical hand movement, sitting down, and standing up for the following experiment.

Sensing coverage. In this experiment, the volunteer is asked to repeat the four activities at increasing distances away from the GNSS receiver, as shown in Figure 19(a). We then plot the sensing accuracy at different distances in Figure 19(b). From the plot, we observe that the overall accuracy remains at 90% as the distance increases to 2 m, but drops quickly to 78.7% when the distance increases to 3 m. The main factor limiting the coverage is the absence of high-elevation angle satellites. When people stand two meters away from the receiver, it can hardly influence the satellites

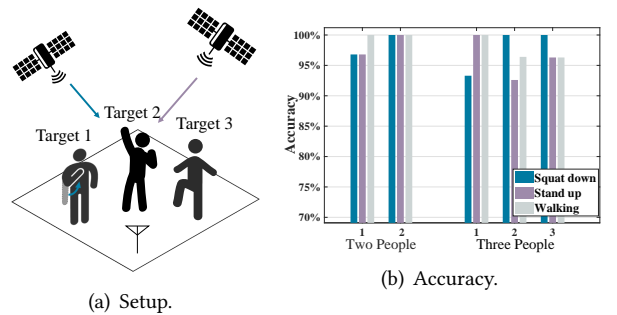


Figure 21: Other volunteer as target.

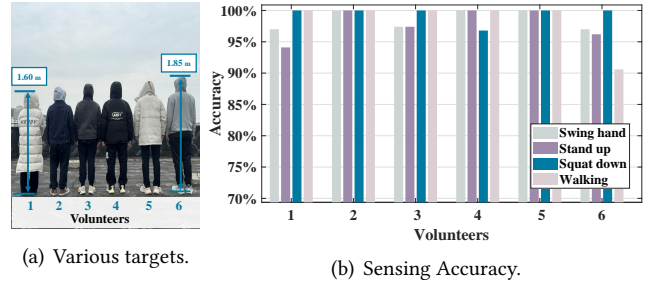
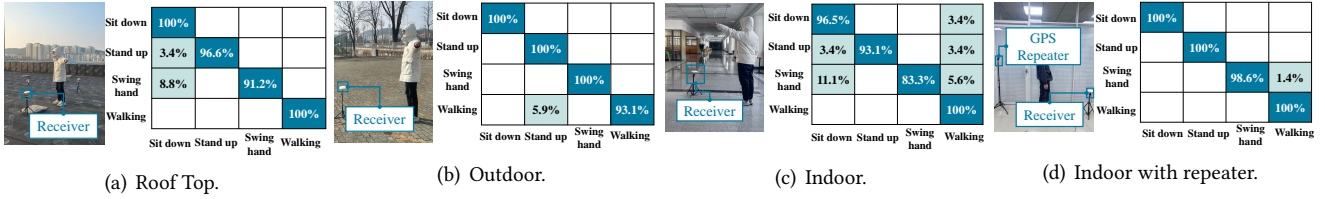
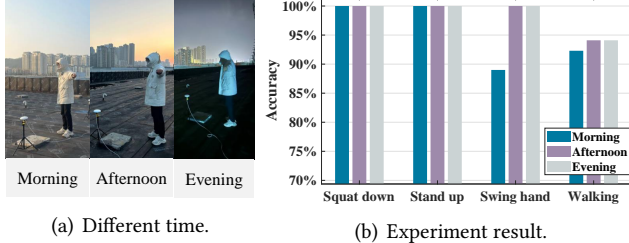
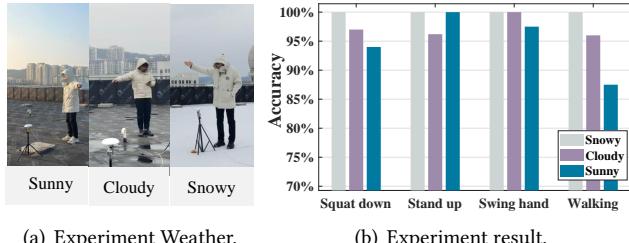


Figure 22: The sensing accuracy with different target sizes.

with an elevation angle above 40 degrees. This results in half of the satellites failing to contribute, leading to a reduction on accuracy. Interestingly, we find that if we increase the vertical distance between the GNSS receiver and the target, for example, by placing the GNSS receiver on the first floor and the target on the second floor, the sensing coverage can increase significantly to ten meters.

Sensing multiple people. We further evaluate the performance of our system in multi-target sensing. We ask three volunteers to participate in two multi-target scenarios with different sensing purposes. For the first scenario, our system only needs to recognize the activity of one volunteer out of the three while considering the other two as interferers. The interferers randomly move their bodies, as illustrated in Figure 20(a). The average sensing accuracy for the target shown in Figure 20(a) is 98.3%. Due to the considerable number of satellites (normally twenty to thirty GNSS satellites) above the target and interferers, there almost always exist GPS signal channels that are influenced only by the target and not by the interferers. Our system can utilize these clean signal channels to mitigate the influence of surrounding interferers on sensing.

In the second scenario, GPSense takes all three volunteers as the sensing targets. We ask the three volunteers to simultaneously perform the four aforementioned activities as illustrated in Figure 21(a), and the sensing performance is shown in Figure 21(b). The average recognition accuracy is 98.9% when two people concurrently perform different gestures, and when the number of people is increased to 3, the average accuracy is still at 97.2%. This is because the large

**Figure 23: The sensing accuracy at different locations.****Figure 24: The sensing accuracy at different times.****Figure 25: The sensing accuracy in different weathers.**

number of distributed satellites enables our system to pick satellite signals only affected by one single target, making simultaneously sensing multiple targets possible.

5.6 System Robustness

In this section, we evaluate the robustness of the proposed system against target variations, diverse experiment environments (both indoor and outdoor), different time of the day, and various weather conditions. Similar to the previous experiment, we select four representative human activities for recognition.

Impact of human diversity. Based on the proposed models, the size of the human target may influence the system performance. We conduct experiments involving 6 volunteers with heights ranging from 160 cm to 185 cm, as detailed in Figure 22(a) to repeat the four activities: walking, vertical hand movement, sitting down, and standing up near the GNSS receiver. Each volunteer repeats each activity 50 times, and we use one sample of each movement collected from the 180 cm volunteer as the reference sample for all targets. The sensing accuracies for each target are detailed in Figure 22(b), from which we can observe that the overall accuracy for all targets is 98.6%. This result demonstrates that the human diversity has little impact on our system, as the signal patterns remain consistent.

Sensing at different places. One advantage of our system is that the pervasive GNSS signals are accessible almost everywhere on Earth. We choose four different experiment environments: on the rooftop of a building, outdoors in a park, indoors with open windows (with weak GPS signals [50]), and in a confined room with a GPS repeater, as shown in Figure 23, to evaluate the sensing performance. In each environment, we instruct a volunteer to repeat the four different activities 50 times. As shown in Figure 23, the average sensing accuracies for the four environments are 98.3%, 96.9%, 93.2%, and 99.7%, respectively. The sensing accuracy in the third environment, i.e., indoor with window-leaked GPS signals, is slightly lower. This is because the building obstructs most of the GNSS signals. To enhance the sensing capability of our system in indoor environments, we can deploy a low-cost GPS repeater as demonstrated in the fourth environment.

Impact of different time. Another advantage of GPSense is that GNSS satellites transmit signals 24/7, ensuring that the system's sensing service is accessible any time. As illustrated in Figure 24(a), the volunteer is instructed to perform four different activities at three different time during the same day. We take one sample for each movement in the afternoon as the reference sample for all the tests. The experiment results are presented in Figure 24(b), from which we observe consistent sensing accuracies at different time (95.3%, 98.5%, 98.5%). Even though the positions of satellites change at different time, the large number of satellites in space ensures that there are always satellites near to position of the satellite when we collected the reference sample. Thus, different time of the day has little impact on our system.

Impact of different weather conditions. Different from wireless signals used in existing sensing systems, such as Wi-Fi, GPS signals are influenced by weather conditions due to the extremely long transmission distances. Thus, we test the influence of different weather conditions on the performance of our system. As illustrated in Figure 25(a), the volunteer performs four different activities under three different weather conditions: sunny, cloudy, and rainy. We take one sample for each movement under the sunny weather as the reference sample for all the tests. Figure 25(b) shows the corresponding experiment results, and the average sensing accuracy under these three weather conditions is 100%, 95.9%, and 94.7%. We find that weather conditions have little

influence on our sensing system since the signal reconstruction process in Section 3 also mitigates the effects caused by weather conditions.

6 DISCUSSION

Other satellites. Our system is designed to leverage wireless signals emitted by satellites within the Global Navigation Satellite System (GNSS), specifically the GPS satellite, for wireless sensing applications. Additionally, we assess the performance of our system across various GNSS satellites, including BeiDou and Galileo. Remarkably, our findings indicate negligible performance differences when utilizing signals from different navigation systems, demonstrating the system's versatility and robustness. In addition to GNSS satellites, various other satellites, including communication satellites like Starlink and TV satellites, continually transmit wireless signals to Earth. We posit that the novel sensing modality we propose can be adapted for the wireless signals transmitted by these satellites through appropriate adjustments in signal processing methodologies.

Fine-grained movement. The current system can recognize ten distinct human activities involving arm/leg or torso movement, characterized by relatively large reflection/diffraction areas. However, detecting subtle fine-grained activities like finger drawing or typing poses a challenge. Due to the significantly weak GPS signals received at the GPS receiver, about -30 dB weaker than Wi-Fi signals, variations in signals induced by these movements may be obscured by Line-of-Sight (LOS) signals and ambient noise. Interestingly, we find the stability of GPS signal frequency and phase, compared to commercial wireless communication devices. Thus, extracting signal variations from fine-grained movements is plausible through advanced receiver hardware design and machine learning methods.

7 RELATED WORK

Wireless sensing. In recent studies, researchers have employed wireless signals, including Wi-Fi [13, 34], UWB [16, 46], and sound [19, 47], for diverse sensing applications. These applications encompass contact-free activity recognition [29], vital signs monitoring [33], and indoor localization [20]. Nevertheless, a majority of sensing systems necessitate a dedicated signal transmitter, such as mmWave [51], or adversely impact the original communication functionality, exemplified by Wi-Fi [42]. In efforts to obviate the need for a dedicated sensing signal, alternative approaches have been explored, such as leveraging signals emanating from LTE towers [9] and signals leaked from power lines [6]. GPSense first time utilizes the pervasive GPS signals emitted from the satellite to conduct wireless sensing, which eliminates

the need for a dedicated signal transmitter and avoids any impact on the communication band.

GPS application. GPS signals were originally designed to provide global positioning services for electronic devices. Presently, billions of electronic devices leverage these signals to calculate their positions using the triangulation method [18]. Recent efforts are mainly engaged in enhancing the accuracy and coverage of GPS, fortifying robustness against environmental factors in urban canyon [4, 23], and facilitating indoor positioning [7, 25, 50]. Beyond their primary function for positioning and navigation, researchers have harnessed GPS signals for GPS precise point positioning (PPP) based remote sensing and mapping applications, including atmospheric monitoring [14, 35] and driver behavior analyzing on GPS records [49]. Diverging from technologies reliant on precision GPS localization, our approach facilitates innovative wireless sensing applications through the analysis of interactions between sensing targets and GPS signals. These applications encompass respiration monitoring, contact-free activity recognition, and device-free tracking and localization.

Diffraction model. The Keller Geometrical Theory of Diffraction (GTD) elucidates the diffraction phenomenon arising when an energy wave impinges upon an edge [15]. Notably, recent research endeavors involve the design of a meta-surface composed of small metal plates functioning as diffraction edges to exert control over RF signals, aligning with the principles of the Keller Cone [27]. Furthermore, researchers employ the diffraction model for the purpose of detecting letters concealed behind a wall using RF signals [28]. In contrast to existing works, our approach utilizes the diffraction model to systematically analyze the influence of moving objects on transmitted GPS signals, thereby enhancing the system's sensing capabilities.

8 CONCLUSION

In this work, we introduce the very first wireless sensing system based on GPS (GNSS) signals from satellites. By reconstructing the signals based on reported measurements from commercial GNSS receivers, we make GPS signals available for sensing. Then, two sensing models are established using the unique feature of GPS signals: their extremely long transmission distance. Lastly, we propose the concept of distributed sensing and fuse GPS signals from multiple satellites to improve sensing capability. GPSense can be implemented on commercial GNSS receivers to achieve various meaningful applications and also provide a new sensing modality to bridge the gap between laboratory setups and real-life usage for wireless sensing technology. We also believe the proposed methods lay a foundation for future distributed sensing systems with satellites in the broad space.

REFERENCES

- [1] Alibaba. 2024. Car Mobile Navigation GPS Signal Enhancement Amplifier Antenna GPS Amplifier and GPS Repeater.
- [2] Florian Bousquet. 2017. Great solution for GPS sports watches.
- [3] Christina Chacour, Mehdi Naderi Soorki, Walid Saad, Mehdi Bennis, Petar Popovski, and Mérouane Debbah. 2022. Seven defining features of terahertz (THz) wireless systems: A fellowship of communication and sensing. *IEEE Communications Surveys & Tutorials* 24, 2 (2022), 967–993.
- [4] Kongyang Chen and Guang Tan. 2018. BikeGPS: Accurate localization of shared bikes in street canyons via low-level GPS cooperation. In *Proceedings of the 16th Annual International Conference on Mobile Systems, Applications, and Services*. 150–162.
- [5] Mostafa Zaman Chowdhury, Md Shahjalal, Shakil Ahmed, and Yeong Min Jang. 2020. 6G wireless communication systems: Applications, requirements, technologies, challenges, and research directions. *IEEE Open Journal of the Communications Society* 1 (2020), 957–975.
- [6] Minhao Cui, Binbin Xie, Qing Wang, and Jie Xiong. 2023. DancingAnt: Body-empowered Wireless Sensing Utilizing Pervasive Radiations from Powerline. In *Proceedings of ACM MobiCom*. 232–244.
- [7] Huixin Dong, Yirong Xie, Xianan Zhang, Wei Wang, Xinyu Zhang, and Jianhua He. 2023. GPSMirror: Expanding Accurate GPS Positioning to Shadowed and Indoor Regions with Backscatter. In *Proceedings of the 29th Annual International Conference on Mobile Computing and Networking*. 1–15.
- [8] Werner Enderle, Francesco Gini, Henno Boomkamp, Joel JK Parker, Benjamin W Ashman, Bryan W Welch, Mick Koch, and O Scott Sands. 2018. Space user visibility benefits of the multi-GNSS Space Service Volume: An internationally-coordinated, global and mission-specific analysis. In *Proceedings of the 31st international technical meeting of the satellite division of the institute of navigation (ION GNSS+ 2018)*. 1191–1207.
- [9] Yuda Feng, Yaxiong Xie, Deepak Ganesan, and Jie Xiong. 2021. LTE-based pervasive sensing across indoor and outdoor. In *Proceedings of the 19th ACM Conference on Embedded Networked Sensor Systems*. 138–151.
- [10] Ruiyang Gao, Mi Zhang, Jie Zhang, Yang Li, Enze Yi, Dan Wu, Leye Wang, and Daqing Zhang. 2021. Towards position-independent sensing for gesture recognition with Wi-Fi. *Proceedings of the ACM on Interactive, Mobile, Wearable and Ubiquitous Technologies* 5, 2 (2021), 1–28.
- [11] Tianbo Gu, Zheng Fang, Zhicheng Yang, Pengfei Hu, and Prasant Mohapatra. 2019. Mmsense: Multi-person detection and identification via mmwave sensing. In *Proceedings of the 3rd ACM Workshop on Millimeter-wave Networks and Sensing Systems*. 45–50.
- [12] Philipp Hillger, Janusz Grzyb, Ritesh Jain, and Ullrich R Pfeiffer. 2018. Terahertz imaging and sensing applications with silicon-based technologies. *IEEE Transactions on Terahertz Science and Technology* 9, 1 (2018), 1–19.
- [13] Wenjun Jiang, Hongfei Xue, Chenglin Miao, Shiyang Wang, Sen Lin, Chong Tian, Srinivasan Murali, Haochen Hu, Zhi Sun, and Lu Su. 2020. Towards 3D human pose construction using wifi. In *26th Annual International Conference on Mobile Computing and Networking (MobiCom)*. ACM, 1–14.
- [14] Shuanggen Jin and Attila Komjathy. 2010. GNSS reflectometry and remote sensing: New objectives and results. *Advances in Space Research* 46, 2 (2010), 111–117.
- [15] Joseph B Keller. 1962. Geometrical theory of diffraction. *Josa* 52, 2 (1962), 116–130.
- [16] Derek Ka-Hei Lai, Li-Wen Zha, Tommy Yau-Nam Leung, Andy Yiu-Chau Tam, Bryan Pak-Hei So, Hyo-Jung Lim, Daphne Sze Ki Cheung, Duo Wai-Chi Wong, and James Chung-Wai Cheung. 2023. Dual ultra-wideband (UWB) radar-based sleep posture recognition system: Towards ubiquitous sleep monitoring. *Engineered Regeneration* 4, 1 (2023), 36–43.
- [17] Richard B Langley. 1997. GPS receiver system noise. *GPS world* 8, 6 (1997), 40–45.
- [18] Alfred Leick, Lev Rapoport, and Dmitry Tatarnikov. 2015. *GPS satellite surveying*. John Wiley & Sons.
- [19] Dong Li, Shirui Cao, Sungsoon Ivan Lee, and Jie Xiong. 2022. Experience: practical problems for acoustic sensing. In *Proceedings of the 28th Annual International Conference on Mobile Computing And Networking*. 381–390.
- [20] Xiang Li, Shengjie Li, Daqing Zhang, Jie Xiong, Yasha Wang, and Hong Mei. 2016. Dynamic-MUSIC: Accurate device-free indoor localization. In *Proceedings of the 2016 ACM international joint conference on pervasive and ubiquitous computing*. 196–207.
- [21] Haipeng Liu, Yuheng Wang, Anfu Zhou, Hanyue He, Wei Wang, Kunpeng Wang, Peilin Pan, Yixuan Lu, Liang Liu, and Huadong Ma. 2020. Real-time arm gesture recognition in smart home scenarios via millimeter wave sensing. *Proceedings of the ACM on interactive, mobile, wearable and ubiquitous technologies* 4, 4 (2020), 1–28.
- [22] Jian Liu, Hongbo Liu, Yingying Chen, Yan Wang, and Chen Wang. 2019. Wireless sensing for human activity: A survey. *IEEE Communications Surveys & Tutorials* 22, 3 (2019), 1629–1645.
- [23] Xiaochen Liu, Suman Nath, and Ramesh Govindan. 2018. Gnome: A practical approach to NLOS mitigation for GPS positioning in smartphones. In *Proceedings of the 16th Annual International Conference on Mobile Systems, Applications, and Services*. 163–177.
- [24] Gemma Murray, William Harper, and Curtis Wilson. 2010. Huygens, Wren, Wallis, and Newton on Rules of Impact and Reflection. In *Vanishing matter and the Laws of motion*. Routledge, 167–206.
- [25] Shahriar Nirjon, Jie Liu, Gerald DeJean, Bodhi Priyantha, Yuzhe Jin, and Ted Hart. 2014. COIN-GPS: Indoor localization from direct GPS receiving. In *Proceedings of the 12th annual international conference on Mobile systems, applications, and services*. 301–314.
- [26] Kai Niu, Fusang Zhang, Jie Xiong, Xiang Li, Enze Yi, and Daqing Zhang. 2018. Boosting fine-grained activity sensing by embracing wireless multipath effects. In *ACM International Conference on emerging Networking EXperiments and Technologies (CONEXT)*. ACM, 139–151.
- [27] Anurag Pallaprolu, Winston Hurst, Sophia Paul, and Yasamin Mostofi. 2023. I Beg to Diffract: RF Field Programming With Edges. In *Proceedings of the 29th Annual International Conference on Mobile Computing and Networking*. 1–15.
- [28] Anurag Pallaprolu, Belal Korany, and Yasamin Mostofi. 2022. Wifftract: a new foundation for RF imaging via edge tracing. In *Proceedings of the 28th Annual International Conference on Mobile Computing And Networking*. 255–267.
- [29] Yili Ren, Zi Wang, Sheng Tan, Yingying Chen, and Jie Yang. 2021. Winect: 3d human pose tracking for free-form activity using commodity wifi. *ACM on Interactive, Mobile, Wearable and Ubiquitous Technologies (IMWUT)* 5, 4 (2021), 1–29.
- [30] Raphael Stauffer, Roland Hohensinn, ID Herrera Pinzón, Gregor Moeller, Yuanxin Pan, Grzegorz Kłopotek, Benedikt Soja, Elmar Brockmann, and Markus Rothacher. 2023. Estimation of tropospheric parameters with gnss smartphones in a differential approach. *Measurement Science and Technology* 34, 9 (2023), 095126.
- [31] U-blox. 2011. Meizu high-definition smartphone for China includes u-blox GPS.
- [32] U-blox. 2015. NEO-M8: U-blox M8 concurrent GNSS modules.
- [33] Fengyu Wang, Feng Zhang, Chenshu Wu, Beibei Wang, and KJ Ray Liu. 2020. Respiration tracking for people counting and recognition. *IEEE Internet of Things Journal* 7, 6 (2020), 5233–5245.

- [34] Hao Wang, Daqing Zhang, Junyi Ma, Yasha Wang, Yuxiang Wang, Dan Wu, Tao Gu, and Bing Xie. 2016. Human respiration detection with commodity WiFi devices: Do user location and body orientation matter?. In *Proceedings of the 2016 ACM international joint conference on pervasive and ubiquitous computing*. 25–36.
- [35] Tianlin Wang, Christopher S Ruf, Scott Gleason, Andrew J O'Brien, Darren S McKague, Bruce P Block, and Anthony Russel. 2021. Dynamic calibration of GPS effective isotropic radiated power for GNSS-reflectometry earth remote sensing. *IEEE Transactions on Geoscience and Remote Sensing* 60 (2021), 1–12.
- [36] Wei Wang, Alex X Liu, and Ke Sun. 2016. Device-free gesture tracking using acoustic signals. In *Proceedings of the 22nd Annual International Conference on Mobile Computing and Networking*. 82–94.
- [37] Xuanzhi Wang, Kai Niu, Jie Xiong, Bochong Qian, Zhiyun Yao, Tairong Lou, and Daqing Zhang. 2022. Placement matters: Understanding the effects of device placement for WiFi sensing. *Proceedings of the ACM on Interactive, Mobile, Wearable and Ubiquitous Technologies* 6, 1 (2022), 1–25.
- [38] Zhijun Wu, Rusan Liu, and Haijuan Cao. 2018. ECDSA-based message authentication scheme for BeiDou-II navigation satellite system. *IEEE Trans. Aerospace Electron. Systems* 55, 4 (2018), 1666–1682.
- [39] Binbin Xie, Minhao Cui, Deepak Ganesan, Xiangru Chen, and Jie Xiong. 2023. Boosting the Long Range Sensing Potential of LoRa. In *Proceedings of the 21st Annual International Conference on Mobile Systems, Applications and Services*. 177–190.
- [40] Binbin Xie, Deepak Ganesan, and Jie Xiong. 2022. Embracing lora sensing with device mobility. In *Proceedings of the 20th ACM Conference on Embedded Networked Sensor Systems*. 349–361.
- [41] Binbin Xie, Jie Xiong, Xiaojiang Chen, and Dingyi Fang. 2020. Exploring commodity rfid for contactless sub-millimeter vibration sensing. In *ACM Conference on Embedded Networked Sensor Systems (SenSys)*. 15–27.
- [42] Kun Yang, Xiaolong Zheng, Jie Xiong, Liang Liu, and Huadong Ma. 2022. Wilmg: pushing the limit of WiFi sensing with low transmission rates. In *2022 19th Annual IEEE International Conference on Sensing, Communication, and Networking (SECON)*. IEEE, 1–9.
- [43] Youwei Zeng, Dan Wu, Jie Xiong, Jinyi Liu, Zhaopeng Liu, and Daqing Zhang. 2020. MultiSense: Enabling multi-person respiration sensing with commodity wifi. *Proceedings of the ACM on Interactive, Mobile, Wearable and Ubiquitous Technologies* 4, 3 (2020), 1–29.
- [44] Youwei Zeng, Dan Wu, Jie Xiong, Enze Yi, Ruiyang Gao, and Daqing Zhang. 2019. FarSense: Pushing the range limit of WiFi-based respiration sensing with CSI ratio of two antennas. *Proceedings of the ACM on Interactive, Mobile, Wearable and Ubiquitous Technologies* 3, 3 (2019), 1–26.
- [45] Daqing Zhang, Fusang Zhang, Dan Wu, Jie Xiong, and Kai Niu. 2021. Fresnel zone based theories for contactless sensing. *Contactless Human Activity Analysis* (2021), 145–164.
- [46] Fusang Zhang, Zhaoxin Chang, Jie Xiong, Junqi Ma, Jiazhi Ni, Wenbo Zhang, Beihong Jin, and Daqing Zhang. 2023. Embracing Consumer-level UWB-equipped Devices for Fine-grained Wireless Sensing. *ACM on Interactive, Mobile, Wearable and Ubiquitous Technologies (IMWUT)* 6, 4 (2023), 1–27.
- [47] Fusang Zhang, Zhi Wang, Beihong Jin, Jie Xiong, and Daqing Zhang. 2020. Your Smart Speaker Can "Hear" Your Heartbeat! *Proceedings of the ACM on Interactive, Mobile, Wearable and Ubiquitous Technologies* 4, 4 (2020), 1–24.
- [48] Fusang Zhang, Jie Xiong, Zhaoxin Chang, Junqi Ma, and Daqing Zhang. 2022. Mobi2Sense: empowering wireless sensing with mobility. In *Proceedings of the 28th Annual International Conference on Mobile Computing And Networking*. 268–281.
- [49] Yanning Zhao, Toshiyuki Yamamoto, and Takayuki Morikawa. 2018. An analysis on older driver's driving behavior by GPS tracking data: Road selection, left/right turn, and driving speed. *Journal of traffic and transportation engineering (English edition)* 5, 1 (2018), 56–65.
- [50] Heng Zhou and Takuya Maekawa. 2023. GPS-assisted Indoor Pedestrian Dead Reckoning. *Proceedings of the ACM on Interactive, Mobile, Wearable and Ubiquitous Technologies* 6, 4 (2023), 1–36.
- [51] Juncen Zhu, Jianrong Cao, Yanni Yang, Wei Ren, and Huizi Han. 2023. mmDrive: Fine-Grained Fatigue Driving Detection Using mmWave Radar. *ACM Transactions on Internet of Things* (2023).
- [52] Yongpan Zou, Jiang Xiao, Jinsong Han, Kaishun Wu, Yun Li, and Lionel M Ni. 2016. Grfid: A device-free rfid-based gesture recognition system. *IEEE Transactions on Mobile Computing* 16, 2 (2016), 381–393.

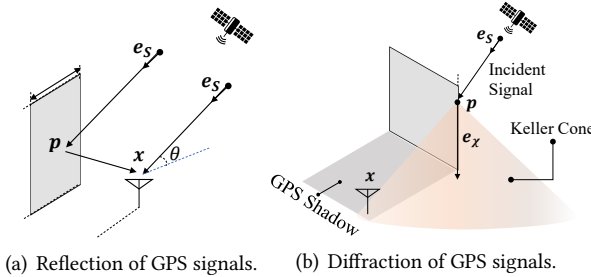


Figure 26: Interaction between the sensing target and the GPS signals.

APPENDIX: SIGNAL REFLECTION AND DIFFRACTION

Reflection Model. As illustrated in Figure 26 (a), if a GPS receiver is fixed at location x , the GPS signal when arriving x from the LoS can be represented as

$$S_{LoS}(x) = \sqrt{P_s} e^{j\phi}, \quad (11)$$

where $\sqrt{P_s}$ is the signal strength of the GPS signals when reaching the ground. If a surface at location p reflects the GPS signal to the GPS receiver, the signal reflected to the receiver can be expressed by

$$S_{Reflect}(x, p) = \frac{\sqrt{P_s}}{4\pi||x - p||^2} e^{j\phi + j2\pi(||(x-p) \cdot e_s|| + ||x-p||)/\lambda}, \quad (12)$$

where we assume the signal strength arriving at p is also $\sqrt{P_s}$ ³, then it attenuate follow the Huygens Law [24] after reflection with attenuation rate $\frac{1}{4\pi||x - p||^2}$. λ is the wavelength of the GPS signals, where $\lambda \approx 19.0$ cm for GPS L1 band signals and 25.0 cm for GPS L5 band signals.

In this situation, the GPS receiver will receive a combination of GPS signals from the LoS and reflect from the sensing target. Hence the signal received can be obtained as

$$S(t) = S_{Reflected} + S_{LoS}. \quad (13)$$

Diffraction Model. When a wave is incident on an edge, a cone of outgoing rays will occur according to Keller's Geometrical Theory of Diffraction (GTD) [15]. The angle of the cone is equal to the angle between the incident ray and the edge. This cone is known as the Keller cone. Figure 26 show samples of edge interaction with GPS signals and the resulting Keller cone. The angle of the cone is equal to the angle between the incident wave and the edge.

As illustrated in Figure 26 (a), consider a single GPS receiver is placed at the location x , the signal from the LoS can also expressed with the above Equation (11). However,

³The GPS signals reaching both the target and the GPS receiver exhibit identical strength, considering their close proximity in comparison to the considerably extensive propagation distance.
different from the reflection model that the LoS always exists, the LoS signal will be absent when the receiver is fixed in the shadow of the sensing target. Hence, the signal from LoS can be expressed as

$$S_{LoS} = \begin{cases} \sqrt{P_s} e^{j\phi}, & \text{LoS exist} \\ 0, & \text{No LoS} \end{cases} \quad (14)$$

The shadow area can be calculated with the size and the incident angle of the GPS signals. Then assuming the GPS signal gets diffracted at a target edge located at p with direction e_χ , the complex field of diffraction at the edge element can be expressed by

$$S_{cone}(x, p, e_\chi) = \frac{\sqrt{P_s} e^{j\phi + 2\pi((x-p) \cdot e_s + ||x-p||/\lambda)}}{2\pi\sqrt{1 - ||e_s \cdot e_\chi||^2}||x - p||} I(p, e_s, e_\chi) \quad (15)$$

where $\sqrt{P_s}$ represents the signal strength of GPS signals when reaching ground, $\frac{1}{2\pi\sqrt{1 - ||e_s \cdot e_\chi||^2}||x - p||}$ is the signal strength attenuation rate according to the GTD theory. $I(p, e_s, e_\chi)$ represents the reflect signal strength, when the receiver at the Keller Cone it equals to 1, else equal to 0. Hence we can obtain the received signal as

$$S(t) = S_{cone} + S_{LoS} \quad (16)$$